changes at the surfactant-water interface. One possibility is that the growing crystals retain a hydration layer together with adsorbed surfactant such that there is a net migration of DDAB molecules toward sites of crystal growth. Therefore, the crystals would no longer be confined to the space delineated by the original water-filled conduits but reshape the microstructure through dynamic changes in the structure of the microemulsion. Although this seems a feasible mechanism in the viscous medium of the liquid oils, it is less obvious that such changes should be associated with microemulsions dispersed in frozen oil. One explanation is that oil molecules associated with the surfactant tails retain some local mobility, although the bulk molecules are frozen. With regard to the construction of the reticulated framework, this construction is probably facilitated by the needle-like morphology of the HAP crystals. This morphology serves to provide effective interlinking and interlocking of the architecture at relatively early stages of formation. Indeed, analogous experiments with CdS, which does not adopt an acicular habit, failed to produce macroporous materials.

Finally, reticulated biominerals, such as corals, have been exploited as biological implants because the macroporosity facilitates intergrowth, vasculization, and the resorption of calcified tissue (*14*). Although the pore size of the reticulated HAP material reported here is possibly too small to allow extensive vasculization, osteoclastic activity and biocompatibility could be expected. In addition, replication of the unperturbed nanoscale microstructure of the DDAB bicontinuous phase might be achieved by minimizing the crystallization forces inherent in systems comprising large crystals such as HAP. Further investigations involving this approach in the synthesis and crystal tectonics of nanoscale cluster materials (for example, CdS) and extended network structures of covalently linked materials (for example, aluminosilicates) are currently being conducted.

REFERENCES AND NOTES

1. S. Mann, *Nature* **365**, 499 (1993).
2. L. Addadi and S. Weiner, *Angew. Chem. Int. Ed. Eng.* **31**, 153 (1992); S. Mann, *J. Chem. Soc. Dalton Trans.* **1993**, 1 (1993).
3. S. Mann *et al.*, *Science* **261**, 1286 (1993), and references therein.
4. C. T. Kresge *et al.*, *Nature* **359**, 710 (1992); A. Monnier *et al.*, *Science* **261**, 1299 (1993).
5. The phase behavior and microstructure of disordered open connected bicontinuous microemulsions have been characterized in numerous studies involving conductivity [S. H. Chen *et al.*, *J. Phys. Chem.* **95**, 7427 (1991)], viscosity (F. D. Blum *et al.*, *ibid.* **89**, 711 (1985)], nuclear magnetic resonance spectroscopy [R. Skurveit *et al.*, *J. Colloid Interface Sci.* **152**, 205 (1992)], fluorescence (*11*), and small angle neutron [J. Eastoe *et al.*, *Langmuir* **8**, 1505 (1992)] or x-ray (T. N. Zemb *et al.*, *J. Phys. Chem.* **91**, 3814 (1987)] scattering measurements.
6. A metastable solution of calcium phosphate was prepared by the mixing of equal volumes of a 5.0 mM solution of calcium nitrate (or calcium chloride) with a 3.6 mM solution of potassium dihydrogen phosphate, and the pH was adjusted to 7.4 by 0.1 M NaOH. In the absence of a microemulsion phase, the onset of calcium phosphate precipitation from this solution occurred within 15 min at room temperature. In a typical experiment, 1.5 cm^3 of this solution was added dropwise to 2.5 cm^3 of a rapidly stirred oil-surfactant mixture at room temperature. Bicontinuous microemulsions formed from a range of oil-water-surfactant compositions were studied (Table 1). In each case, the formation of the bicontinuous phase was accompanied by the formation of an optically clear mixture. DDAB [$(C_{12}H_{25})_2(CH_3)_2NBr$] and the alkane oils dodecane ($C_{12}H_{26}$), tetradecane ($C_{14}H_{30}$), and hexadecane ($C_{16}H_{34}$) were obtained from Aldrich Chemical. The oils were filtered through 0.2-μm membranes before use.
7. Rapid cooling in liquid nitrogen was required to minimize phase changes in the microemulsion system that are known to occur between 5° and 15°C.
8. Freezing points are as follows: dodecane, −9.6°C; tetradecane, +5.9°C; hexadecane, +18.1°C. Mixtures of tetradecane and hexadecane were used (hexadecane does not form bicontinuous microemulsions because of poor penetration of the oil into the surfactant alkyl chains).
9. Bicontinuous microemulsions in dodecane, stored at −25°C, were soft in texture, indicating a supercooled aqueous phase.
10. A few milligrams of extensively washed and dried material was examined by x-ray diffraction with a Debye-Scherrer camera and CuK radiation. Infrared spectra of dried samples were studied with the use of KBr disks with a Nicolet Fourier transform-infrared spectrometer. Samples for scanning electron microscopy and transmission electron microscopy (TEM) were prepared by the mounting of small amounts of the mineralized material extracted after centrifugation and careful washing of the TEM grids with hot hexane followed by air drying. Samples observed by SEM were gold-coated and examined with a Jeol 1200EX electron microscope operating at 120 kV Transmission electron microscopy examination. was conducted with Jeol 1200EX and 2000FX electron microscopes operating at 120 and 200 kV, respectively.
11. V. Chen, G. C. Warr, D. F. Evans, F. G. Prendergast, *J. Phys. Chem.* **92**, 768 (1988).
12. U. Olsson, K. Shinoda, B. Lindman, *ibid.* **90**, 4083 (1986).
13. S. T. Hyde, B. W. Ninham, T. Zemb, *ibid.* **93**, 1464 (1989).
14. R. Holmes *et al.*, *Clin. Orthop.* **188**, 252 (1984).

15. We thank Unilever Research for financial support and T. Douglas for advice with experimental work concerning cadmium sulphide.

14 January 1994; accepted 25 April 1994

The Structural Basis of Sequence-Independent Peptide Binding by OppA Protein

Jeremy R. H. Tame, Garib N. Murshudov, Eleanor J. Dodson, Teresa K. Neil, Guy G. Dodson, Christopher F. Higgins, Anthony J. Wilkinson*

Specific protein-ligand interactions are critical for cellular function, and most proteins select their partners with sharp discrimination. However, the oligopeptide-binding protein of *Salmonella typhimurium* (OppA) binds peptides of two to five amino acid residues without regard to sequence. The crystal structure of OppA reveals a three-domain organization, unlike other periplasmic binding proteins. In OppA-peptide complexes, the ligands are completely enclosed in the protein interior, a mode of binding that normally imposes tight specificity. The protein fulfills the hydrogen bonding and electrostatic potential of the ligand main chain and accommodates the peptide side chains in voluminous hydrated cavities.

In bacteria, periplasmic substrate-binding proteins capture extracellular nutrients and deliver them to membrane-associated complexes that translocate the ligand across the inner membrane and into the cytoplasm (*1*). Several periplasmic binding proteins specific for substrates, such as sulfate, leucine, and maltose, have been characterized in detail. Each consists of two structurally similar domains that engulf the ligand, sequestering it from bulk solvent, by a mechanism that has been likened to a Venus flytrap (*2*). The oligopeptide-binding protein OppA is distinguished from these binding proteins by its broad specificity. It binds peptides (dissociation constant $K_d \approx 10^{-6}$ M) that vary in length from two to five amino acid residues essentially without regard to their side chains; it therefore has many potential ligands, including cell wall peptides of unusual composition and peptide-based antibiotics, yet it excludes single amino acids and related compounds (*3*, *4*). The accommodation of heterogeneous ligands, varying in size, charge, and polarity, within the interior of a protein presents structural and chemical challenges as the stable

J. R. H. Tame, G. N. Murshudov, E. J. Dodson, T. K. Neil, G. G. Dodson, A. J. Wilkinson, Department of Chemistry, University of York, York YO1 5DD, UK.
C. F. Higgins, ICRF Laboratories, Institute of Molecular Medicine, and Nuffield Department of Clinical Biochemistry, University of Oxford, John Radcliffe Hospital, Oxford OX3 9DU, UK.

*To whom correspondence should be addressed.

burial of ligand groups is normally associated with complementary interactions and, therefore, with specificity. The crystal structures of OppA-peptide complexes presented here reveal an enclosed but versatile ligand-binding envelope.

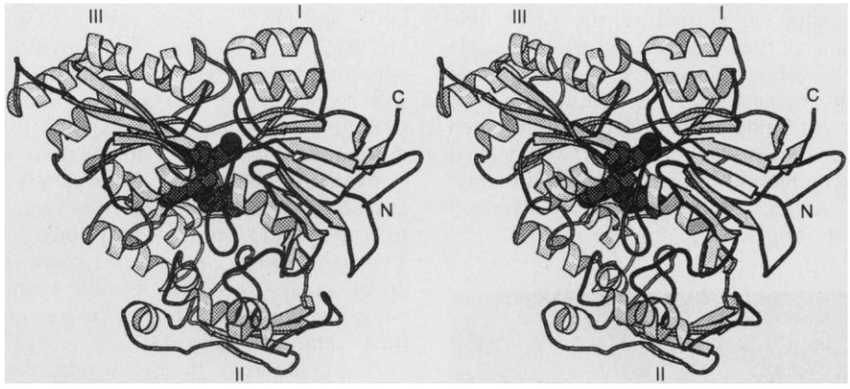

Fig. 1. Stereo ribbon diagram showing the overall topology of the OppA molecule. All atoms of the trilysine ligand are represented as solid spheres. The protein is made up of three domains indicated by the roman numerals I (residues 1 to 44, 169 to 270, and 487 to 517), II (45 to 168), and III (271 to 486). Drawn with the program MOLSCRIPT (*9*).

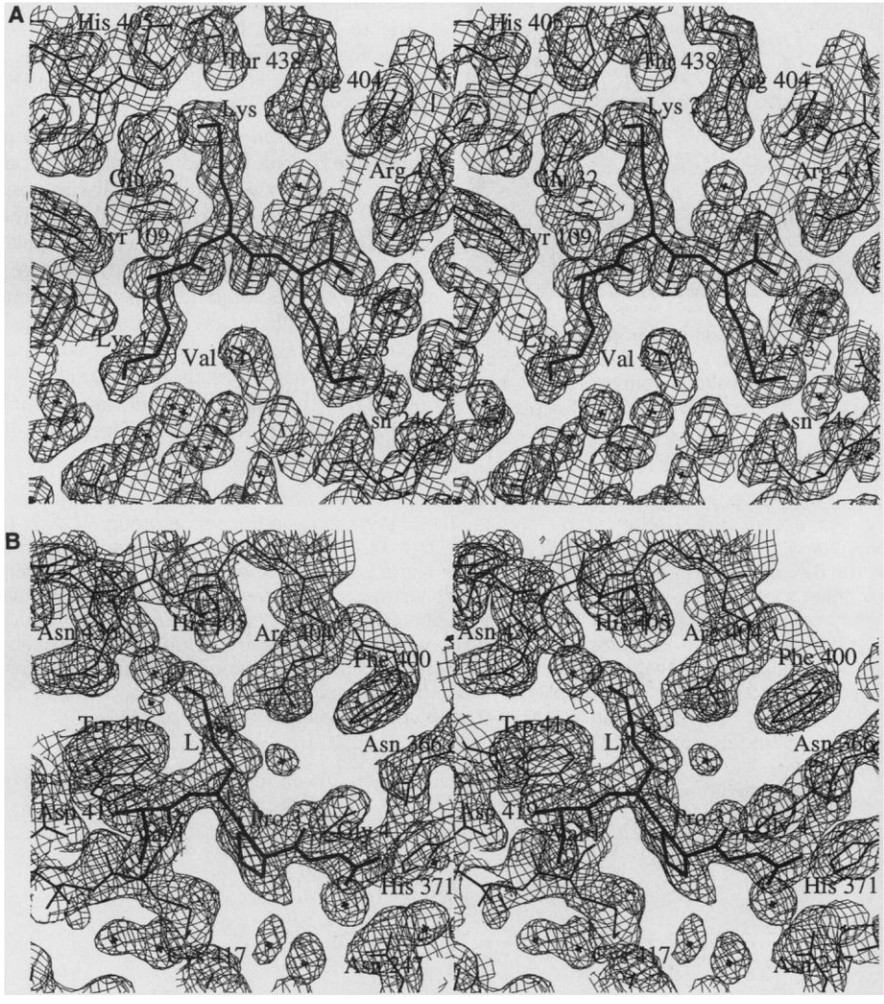

Fig. 2. Stereo view of electron density in the binding pocket of the refined OppA structures together with the modeled peptide ligands (bold lines). The $2F_o - F_c$ electron density, contoured at the 1σ level, is displayed. (**A**) The density is obviously that of the introduced trilysine; (**B**) the nature of the ligand is unknown and has been modeled as Val-Lys-Pro-Gly.

The crystal structure of the liganded form of OppA consists of three domains, each containing a β sheet (Fig. 1 and Table 1). Two of the domains present surfaces that enclose the ligand and are structurally analogous to those present in other periplasmic substrate-binding proteins (*2*). These two domains (I and III in Fig. 1) are linked by two segments that allow them to open and close. Despite this structural similarity, there is no sequence similarity between OppA and other periplasmic binding proteins of known structure. Domain II has no counterpart among these periplasmic substrate-binding proteins, and its function is not known. This domain is about 120 amino acid residues in length and accounts for the larger size of OppA (relative molecular mass M_r = 59,000) relative to the other periplasmic binding proteins (M_r = 26,000 to 41,000). It is formed from two β hairpins and makes few contacts with the ligand. A number of bacterial proteins, including dipeptide-, haem-, and nickel-binding proteins, share sequence similarity with OppA over their entire length (*5*), indicating that these proteins also contain an equivalent of domain II.

The structures of two liganded forms of OppA have been determined, the first containing trilysine (Fig. 2A) and the second containing a copurified (presumably heterogeneous) tetrapeptide (Fig. 2B). The peptides are completely buried within the protein (Fig. 3). The interactions of the bound trilysine with the protein can be divided into those of the main chain and those of the peptide side chains. The main chain of the peptide is in an extended conformation and forms parallel and antiparallel β-sheet interactions with residues 32 to 34 and 415 to 417 of OppA that completely satisfy the hydrogen bonding capacity of the peptide backbone (Fig. 4). In addition, the α-amino group of the peptide forms a salt bridge to the Asp^{419} carboxylate group and balances charge. These observations are consistent with the finding that a protonated α-amino group and an unmodified α-peptide bond are major determinants of peptide binding (*6*). Arg^{413} and His^{371} each form a salt bridge with the carboxylate groups of the tri- and tetrapeptide ligands, respectively (Fig. 2). In the tripeptide complex, an acetate ion occupies the site of the COOH-terminal carboxylate group of the tetrapeptide; a second acetate ion, salt bridged to Lys^{307}, indicates a possible binding site for the COOH-terminal carboxylate group of a pentapeptide ligand (Fig. 3). Therefore, OppA achieves tight peptide binding by fulfilling the hydrogen bonding and electrostatic potential of the ligand main chain.

A distinctly different picture obtains for the side chain interactions. Three side chain binding pockets have been identified

in the structure of the trilysine complex. The structure with the copurified heterogeneous peptide (modeled as Val-Lys-Pro-Gly, consistent with the shape of the ligand electron density) (Fig. 2B) permits only a tentative identification of the fourth side chain pocket. The first three side chain pockets are lined by different constellations of functional groups. Each pocket is apolar close to the ligand backbone and expands into a capacious and hydrated cavity surrounded by protein side chains.

The side chains of Val^{34} and the disulfide bridge between Cys^{271} and Cys^{417} are straddled by the peptide ligand and present a nonpolar surface to the first and third ligand side chain β and γ carbons (Fig. 4). The valine and proline side chains at positions 1 and 3 in the tetrapeptide ligand and the aliphatic portion of the lysine side chains at these positions in the tripeptide pack against this surface to form a local hydrophobic core. The ϵ-amino group of the first lysine of the tripeptide is solvated by an extensive network of well-defined water molecules, which themselves interact with protein side chain amide and hydroxyl groups (Fig. 4).

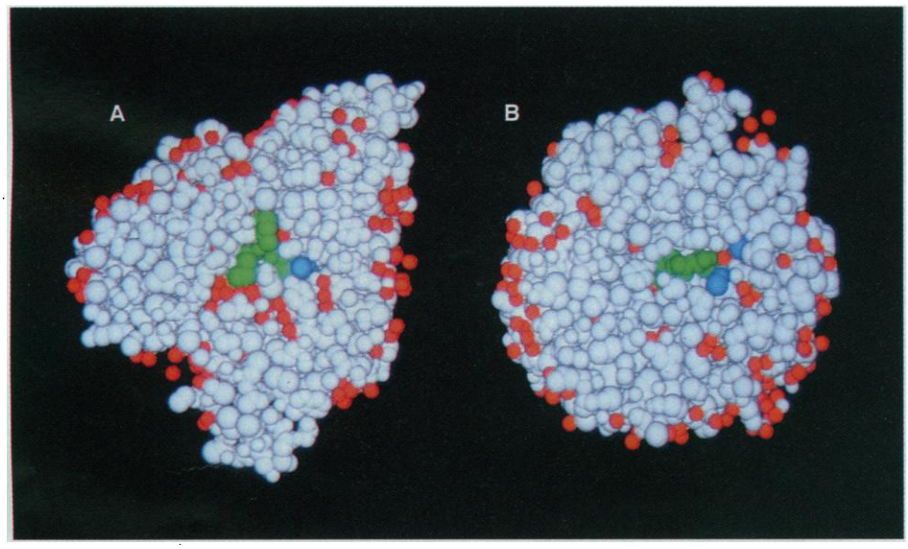

Fig. 3. Orthogonal slices through the OppA-trilysine structure. All protein nonhydrogen atoms are depicted as white van der Waals spheres. Oxygen atoms of solvent water molecules are in red, the ligand is in green, and acetate ions are in blue. The ligand main chain runs from left to right (N to C). In (**A**), the side chains point up and down; in (**B**), they are directed into and out of the plane of the page.

In the second side chain pocket, the apolar collar is formed by Trp^{397}, Trp^{416}, Leu^{401}, and the aliphatic portion of Glu^{32}. The pocket then widens and is flanked by charged side chains indulging in ion pairs; Glu^{32} and His^{405} on one side and Glu^{276} and Arg^{404} on the other. This provides an opportunity for electrostatic interactions with polar ligand side chains, but the strength of these interactions appears to be dissipated by other ionic interactions and by hydration, so that apolar side chains can also be accommodated. The third lysine of trilysine extends into a cavity lined with asparagine amide groups and tyrosine hydroxyl groups with the ligand's ϵ-amino group interacting with one of the cocrystallized acetate ions (Fig. 4).

There are few, if any, strong, direct interactions between OppA and the ligand side chains that could impose specificity (Fig. 4). The hydrogen bonds between OppA and the ligand side chains have poorer geometry than those made with the peptide main chain and are likely to contribute little to binding. Instead, the protein uses large hydrated cavities to accommodate a wide variety of chemical groups. Amide and hydroxyl groups of the protein, together with the enclosed water molecules, serve as adaptable hydrogen bonding groups that can act as donors or acceptors to stabilize positive or negative charges or dipoles on the ligand side chains. In the presence of apolar side chains, these groups can form hydrogen bonds to each other. The number of solvent molecules displaced on binding will adjust according to the ligand size, so that water molecules occupy volume not taken up by ligand side chains. The mechanism by which OppA achieves sequence-independent li-

Table 1. Structure solution. Crystals of OppA, copurified with endogenous peptides (*10*), were grown from 50 mM NaOAc (Ac, acetyl) (pH 5.5), 15% polyethylene glycol 4000, and 1 mM uranyl acetate. These OppA_U crystals have the space group $P2_12_12$ (a = 106.5 Å, b = 74.5 Å, c = 70.0 Å) and contain a single uranium atom at a general position. Data sets were collected on station 9.5 at the Synchrotron Radiation Source Daresbury at two wavelengths around the L_{III} edge of uranium and were used with a CuKα data set (1.54 Å) to calculate multiwavelength anomalous diffraction phases (*11*). These phases produced electron density maps of poor quality. A second crystal form (OppA_L) grows under the same conditions when the endogenous ligand is replaced by trilysine. These crystals have the space group $P2_12_12_1$ (a = 110.6 Å, b = 77.1 Å, c = 72.2 Å) and contain eight uranium atoms. In some crystals (Deriv-1 and Deriv-2), the occupancy of the uranium atoms at some of these sites was lowered, and data from these crystals allowed the calculation of multiple isomorphous replacement phases in the program MLPHARE, which were improved by density modification with SQUASH (*12, 13*). The resultant electron density maps were again of poor quality. Averaging of the maps in the two crystal forms, in the program RAVE (*14*), produced an interpretable map (*15*).

Data set	Device	Resolution (Å)	Intensity (I) ≥ 3σ(I) (%)	Completeness (%)	Unique reflections	Average multiplicity	R_{merge}* (%)	Phasing power†
			OppA_U					
0.72 Å	Mar plate	3.1	93.3	54.1	5,990	3.4	3.7	0.7
0.87 Å	Mar plate	3.1	98.3	42.3	4,458	7.1	2.3	0.8
1.54 Å	Raxis/Xentronics	2.1	85.8	89.7	30,656	2.7	6.7	
			OppA_L					
Native	Raxis	2.1	79.8	70.5	29,289	2.3	5.7	1.5‡
Deriv-1	Xentronics	3.2	90.1	88.1	9,421	9.6	7.8	
Deriv-2	Xentronics	3.0	82.5	87.8	11,056	4.0	7.5	1.5‡
Native (−150°C)	Xentronics	1.8	72.4	83.7	47,801	3.3	5.7	

*$R_{merge} = \Sigma(|I_i - \langle I \rangle|)/\Sigma\langle I \rangle$ †Phasing power = F_H/residual lack of closure error. ‡Deriv-1 has the lowest occupancy of U and was used as the "native" data set in phase calculation (see legend).

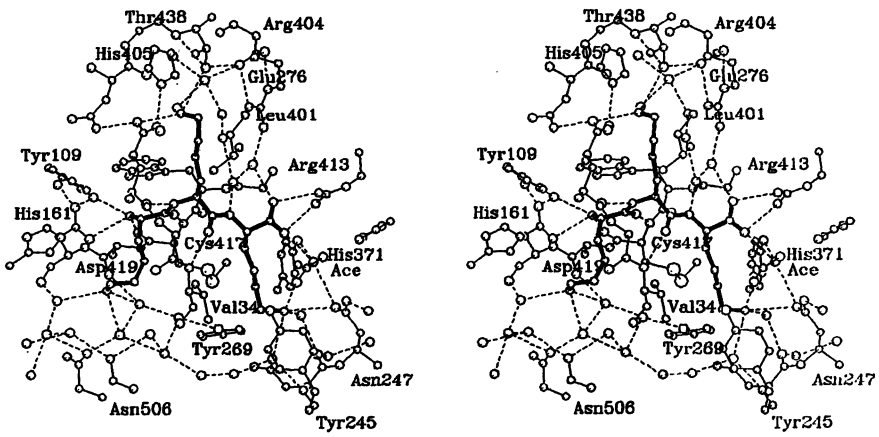

Fig. 4. Stereo diagram showing potential hydrogen bonding and electrostatic interactions (dashed lines) between the trilysine ligand (thicker bonds) and OppA.

gand binding appears, therefore, to be based chiefly on the avoidance of potentially unfavorable interactions with the repertoire of ligand side chains.

The burial of peptide ligands within OppA according to the Venus flytrap mechanism in some sense represents the final stage of a folding process to form a protein with a variable peptide core and a unique surface structure that is efficiently recognized by the membrane components of the transport system. The manner in which OppA accommodates the diverse peptide side chain functional groups is quite distinct from the way this is achieved in major histocompatibility complex molecules and chaperone proteins. In the crystal structures of the latter, the peptide ligands are located on the surfaces of the molecules and many of the side chains are directed into the solvent (*7*).

The covalent coupling of synthetic antibacterial compounds to peptides has proved a successful route to overcoming the problem of membrane impermeability associated with some of these drugs (*4*). This "Trojan horse" approach (*8*) relies on the unusually broad specificity of the oligopeptide permease. Knowledge of the structure of the initial receptor for this transport system, OppA, will be valuable in guiding the design of effective peptide-based antibiotics.

REFERENCES AND NOTES

1. G. F.-L. Ames, *Annu. Rev. Biochem.* **55**, 397 (1986); C. F. Higgins, *Annu. Rev. Cell Biol.* **8**, 67 (1992).
2. F. A. Quiocho, *Curr. Opin. Struct. Biol.* **1**, 922 (1991), and references therein; B.-H. Oh *et al.*, *J. Biol. Chem.* **268**, 11348 (1993); S. L. Mowbray and L. B. Cole, *J. Mol. Biol.* **225**, 155 (1992).
3. J. Payne and C. Gilvarg, *J. Biol. Chem.* **243**, 6292 (1968); C. A. Guyer *et al.*, *J. Bacteriol.* **168**, 775 (1986); E. W. Goodell and C. F. Higgins, *ibid.* **169**, 3861 (1987).
4. B. N. Ames *et al.*, *Proc. Natl. Acad. Sci. U.S.A.* **70**, 456 (1973); T. E. Fickel and C. Gilvarg, *Nature* **241**, 161 (1973); S. M. Hammond *et al.*, *ibid.* **327**, 730 (1987).
5. M. S. Hanson *et al.*, *Infect. Immun.* **60**, 2257 (1992); W. N. Abouhamad *et al.*, *Mol. Microbiol.* **5**, 1035 (1991); C. Navarro *et al.*, *ibid.* **9**, 1181 (1993); E. Olson *et al.*, *J. Bacteriol.* **173**, 234 (1991); R. Tan and M. H. Saier, *Microbiol. Rev.* **57**, 320 (1993).
6. J. Payne and C. Gilvarg, *Adv. Enzymol.* **35**, 187 (1971).
7. P. J. Bjorkman *et al.*, *Nature* **329**, 512 (1987); D. R. Madden *et al.*, *ibid.* **353**, 321 (1991); M. J. Kuehn *et al.*, *Science* **262**, 1234 (1993).
8. C. F. Higgins, *Nature* **327**, 655 (1987).
9. P. J. Kraulis, *J. Appl. Crystallogr.* **24**, 946 (1991).
10. S. P. Tolley *et al.*, *J. Mol. Biol.* **204**, 493 (1988); I. D. Hiles and C. F. Higgins, *Eur. J. Biochem.* **158**, 561 (1986).
11. W. A. Hendrickson, *Science* **254**, 51 (1991); I. D. Glover *et al.*, in preparation.
12. *CCP4: A Suite of Programs for Protein Crystallography* (SERC Daresbury Laboratory, Warrington, UK, 1986).
13. K. D. Cowtan and P. Main, *Acta Crystallogr. D* **49**, 148 (1993).
14. G. J. Kleywegt and T. A. Jones, in preparation.
15. A partial model comprising 461 of the 517 residues was built in the program O [T. A. Jones and M. Kjeldgaard, *O—The Manual* (Uppsala University, Sweden, 1991)]. This model was refined in the program X-PLOR [A. T. Brünger, *X-PLOR Version 2.1* (Yale University, New Haven, CT, 1990)]. Calculated and model-derived phases were combined in the program SIGMAA [R. J. Read, *Acta Crystallogr. A* **42**, 140 (1986)], allowing the remaining residues to be added. Subsequently, the structure was refined independently for the two crystal forms with the program X-PLOR; manual model adjustment was done in the program O; and cycles of least squares refinement were carried out with the program PROLSQ (*12*). The OppA_U structure, which comprises 4550 atoms, including 354 water molecules, two uranium atoms, and the tetrapeptide ligand Val-Lys-Pro-Gly, has a crystallographic *R* factor of 16.7% for all data (29,634 reflections) between 8 and 2.1 Å spacing and root-mean-square (rms) deviations of bond lengths and angles from ideal values of 0.015 Å and 0.037 Å, respectively. The OppA_L structure, which was refined against data collected at −150°C, comprises 4663 atoms, including 432 water molecules, eight uranium atoms, five acetate ions, and the tripeptide Lys-Lys-Lys, and has an *R* factor of 17.3% for all data (47,801 reflections) between 10 and 1.8 Å spacing. The rms deviations in bond lengths and angles from ideality are 0.018 Å and 0.034 Å, respectively.

16. This work was supported by the Medical Research Council, the Science and Engineering Research Council, and the Imperial Cancer Research Fund. C.F.H. is a Howard Hughes International Research Scholar. We would like to thank I. Glover, R. Denny, and P. Moody for assistance in collecting x-ray data and D. Edwards, U. Gileadi, S. Hyde, and S. Mowbray for helpful discussions.

22 February 1994; accepted 25 April 1994

Habitat Fragmentation, Species Loss, and Biological Control

Andreas Kruess* and Teja Tscharntke

Fragmentation of habitats in the agricultural landscape is a major threat to biological diversity, which is greatly determined by insects. Isolation of habitat fragments resulted in decreased numbers of species as well as reduced effects of natural enemies. Manually established islands of red clover were colonized by most available herbivore species but few parasitoid species. Thus, herbivores were greatly released from parasitism, experiencing only 19 to 60 percent of the parasitism of nonisolated populations. Species failing to successfully colonize isolated islands were characterized by small and highly variable populations. Accordingly, lack of habitat connectivity released insects from predator control.

Research in conservation biology analyzes both species richness and the functioning or stability of ecosystems. Modern agricultural methods fragment natural ecosystems; and the subsequent increase in isolation typically results in changes in community structure and function, including loss of species in isolated islands and disruption of the food web (*1*). Communities of herbivorous insects and their natural enemies (such as parasitoids) centered on a single plant species provide a small ecosystem in which the interactions between the organisms can be experimentally analyzed. Insects amount to more than half of all living organisms and

A. Kruess, Zoologisches Institut I, Universität, Kornblumenstrasse 13, D-76128 Karlsruhe, Germany.
T. Tscharntke, FG Agrarökologie, Universität, Waldweg 26, D-37073 Göttingen, Germany.

*To whom correspondence should be addressed.